THE e/K' DIAGRAM. AN APPLICATION OF THE «SLIP MODEL» TO THE POPULATIONAL FAULT ANALYSIS

G. de Vicente (*)

ABSTRACT

The existing problems in the analysis of tectonical evolutions by brittle indicators in areas affected by several phases, as well as the populational analysis methods based on the concepts of eigenvalues and eigenvectors are analyzed, concluding that it is preferable to use methods in which the singularity of each data is not lost, as in the P/T and y/R diagrams.

The «slip model» is developed, introducing the K' factor (e_y/e_z ratio in the strain ellipsoid) and drawing the e/K' and e/Ø diagrams, from which it is possible to analyze the evolutions of type of the strain ellipsoid just from trends and dips of faults.

To study brittle tectonics in a given area it is proposed the use of a combination of methods, and to take into account the data obtained by field geology.

Key words: Brittle tectonics, Faults, Slip model, Strain.

RESUMEN

Se analizan los problemas que presenta el análisis de los marcadores frágiles a la hora de estudiar evoluciones tectónicas en áreas afectadas por varias fases así como los que presentan los métodos de análisis poblacional de fallas basados en el concepto de autovalores y autovectores, concluyendo que resulta preferible utilizar métodos en los que no se pierda la singularidad de cada dato, como son los diagramas P/T e y/R.

Se desarrolla el «modelo de deslizamiento» introduciéndose el factor K' (e_y/e_z del elipsoide de deformación) concluyendo en la construcción de los diagramas e/K' y e/Ø, desde los que resulta posible analizar, sólo con direcciones y buzamientos de fallas, las evoluciones del tipo de elipsoide de deformación.

Se propone que, a la hora de estudiar la tectónica frágil de un área determinada se utilice una combinación de métodos así como que se tengan en cuenta los datos obtenidos de la geología de campo.

Palabras clave: Tectónica frágil, Fallas, Modelo de deslizamiento, Deformación.

de Vicente, G. (1988): The e/K' diagram. An application of the «Slip model» to the populational fault analysis. *Rev. Soc. Geol. España,* 1, (1-2), 97-112.

de Vicente, G. (1988): El diagrama e/k'. Aplicación del «Modelo de deslizamiento» al análisis de poblaciones de fallas. *Rev. Soc. Geol. España,* 1, (1-2), 97-112.

1. INTRODUCTION

To study tectonic evolutions in the brittle field we can focus our attention either in the kinematic indicators (stylolites, joints, veins, faults) in order to define different regimes and sequences, as well as in their populational analysis, mainly of micro or meso-faults and even joints, to deduce the different types of ellipsoids, either of stress (dynamic models) or strain (kinematic models) (McKenzie and Jackson, 1983) that have affected a given area.

When dealing with large data populations apparently is more convenient just to consider the kinematic indicators, since the populational analysis methods seem to be less reliable (Hancock, 1985). This opinion, extended among the tectonicists that are dedicated to the brittle field, may partly be due to the large amount of proposed methods, not all of them useful in common geological situations (for instance the Arthaud's method, 1969), because of the degree of error that usually the microstructural data have, and because some of them are not easily usable (for instance, Aleksandrowski's

(*) Dpto. Geodinámica. Facultad de Ciencias Geológicas. Universidad Complutense. 28040 Madrid (Spain).

method, 1983). On the other hand, to forget about the populational fault analysis means today to forget about a serious trial of quantification in brittle tectonics.

2. PROBLEMS AND LIMITS IN THE STUDY OF KINEMATIC INDICATORS

The brittle microstructures allow us to know, with acceptable degree of error, the location of the axes of stress or strain and qualitatively to know what type of regime we are dealing with. From the spatial relationships temporal tectonic evolutions can be known. An excellent summary of this methodology can be found in Hancock, (1985). However, we shoud avoid the situations of local stresses, and this is not usually easy to get. This can be very evident, for instance in two of the more important brittle kinematic indicators, as the stylolites and veins. It is very common to recognize field situations as those shown in Fig. 1. Close to the end of small faults sometimes can be seen an association of stylolites and veins that shows a local stress field due to the dynamics of the end of the fault itself, that is not related to the regional stress field. The problem is that this situation can be produced in very different scales, and when the distance between the fault and the «non regional stylolite» is large enough the mistake of obtaining more tectonic phases than those that really existed in the studied region can be made. Then, when studying a given area it results very convenient to compare the density diagrams of stylolites and veins in one hand and the fault directions in the other. If in the stylolite diagrams exist maximums, that generally are not the main ones, that coincide with a well marked faulting direction, or the poles in the vein diagrams, are at 90 degrees from the fault directions, we can start thinking of the possibility that those maximums can be due to local situations different from the regional, which has to be tested in the field.

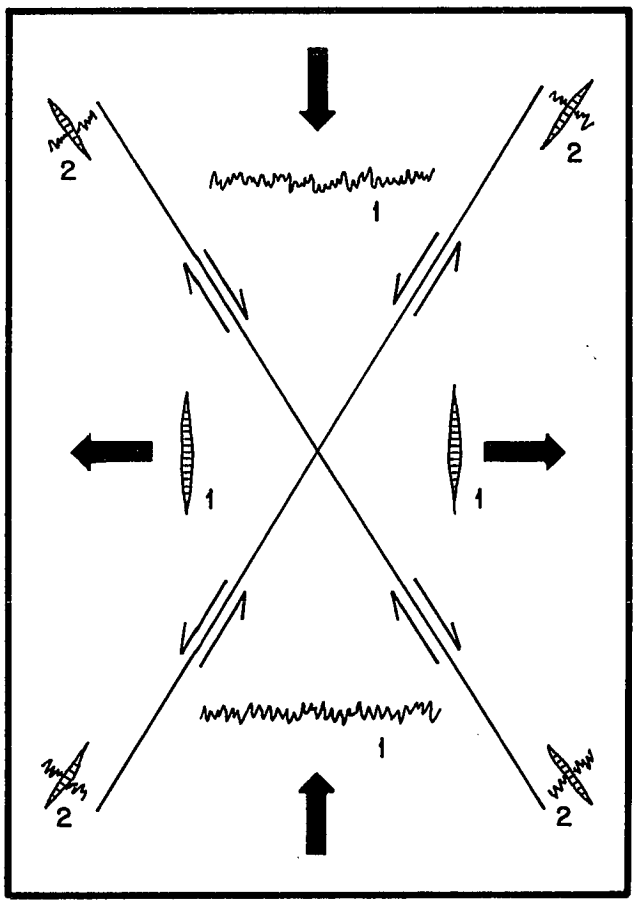

Fig. 1.—Bidimensional diagram showing the relationships among the stylolite and regional veins (1) and local ones (2), in this case related to fault termination.

Fig. 1.—Esquema bidimensional mostrando la relación entre los estilolitos y venas regionales (1) y otros locales (2), en este caso relacionados con la terminación de fracturas.

On the other hand, in the relationships between the microstructures and the stress and strain fields the effect of the intermediate axis of those ellipsoids hasn't been taken into account, since it just has been considered the case of biaxial field or plane strain. We think that considering the effect of that intermediate axis, the spatial relationships between the different types of microstructures can get considerably more complex. Fig. 2 tries to summarize the types of stylolites and veins that theoretically can be produced in all the possible cases of triaxial deformation. It can be seen that when the deformation due to the intermediate axis is big enough it will be possible to get stylolites as well as secondary veins, independent and less developed that the main ones. It results evident that the relationships between the main and secondary markers can be complex. In this way, the same tectonic phase can produce a set of microstructures that can give interpretation errors if they are not considered with enough care.

The situations that we have just shown are logically more frequent in very deformed areas and in those that have had several superimposed tectonic phases. That is the case of the Iberian Range in the east of the Iberian Peninsula, where we have tested the relationships that we have described above.

3. PROBLEMS AND LIMITS OF THE POPULATIONAL ANALYSIS

When we apply the concepts of statistical sampling to the microstructural data, it is often forgotten that this type of data usually have a high «bias error». This type of errors exist because the sample where those data have been gotten from doesn't represent the population but it is chosen with some bias (it is usually measured the showiest fault). This type of errors come from the method used to choose the sample, that usually is far from the simple random sampling, that consists in getting a given number of random samples from a given population of microstructures. This means that, from this point of view, to get useful field data these should be totally random, for instance drawing a mesh in the outcrops; choosing random coordinates, and measuring

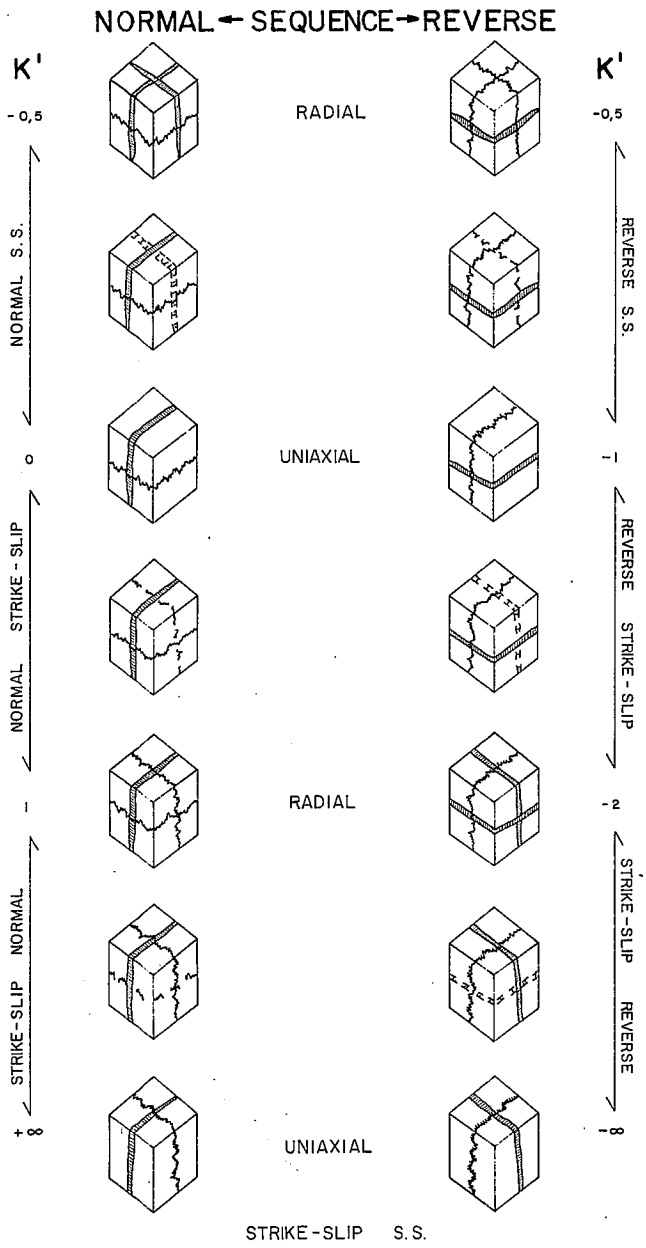

Fig. 2.—Kinds of deformational regimes defined by K' (see text) and the two possible sequences (normal and reverse). They are showed related to the development of stylolitic peaks and tension gashes. Taking into account the intermediate axis, secondary stylolites and veins (dashed) ca be formed in addition to the main ones during the same deformational phase. This will be more obvious when the deformational ellipsoid character is closer to «radial» (two semiaxes with close values).

Fig. 2.—Tipos de regímenes deformacionales, definidos por K' (ver texto) y las dos secuencias posibles (normal e inversa). Se muestran en relación al desarrollo de picos estilolíticos y grietas de tensión. Al tener en cuenta el eje intermedio, se pueden formar, además de los principales, estilolitos y venas secundarios (a trazos), en una misma fase de deformación. Esto resultará más evidente cuando el carácter del elipsoide de deformación sea más cercano a «radial» (dos semiejes con valores próximos).

the microstructures that appear in such a mesh without taking care of their size. This procedure turns to be very complicated to put into practice due to the singularity of the microstructural data. In this regard should be mentioned that the statistical methods developed up to now, mainly based in the concept of eigenvalues and eigenvectors of tensor quantities that are a function of the directional cosines of faults and frictional wear striations, somehow should take into account this type of error. Therefore, it's very common that in a given outcrop there is a predominant direction over the other to which it is really associated (Fig. 3). If we apply a method based on the eigenvectors the deductible direction of the stress or strain ellipsoid will have a tendency to be located closer to the maximum of poles than qualitatively we should be able to deduce, using for instance the minimum dihedral criteria (Fig. 4). Then, there should be «statistical» methods in which the singularity of each data is not lost. In this regard, we should mention two of the many proposed methods.

The first one is the method of the density of compression and extension axes (P/T diagram) (Angelier and Mechler, 1977). It is based on the concept that a fault plane and its striation define four orthogonal dihedral in such a way that in the moment of the movement two of them stay in compression and two in extension. Adding up the extension and the compression areas from a given fault population, it's possible to draw the percentage of the common areas in extension and in compression. This method constitutes an excellent first approximation to the study of a given population. On the other hand, it is qualitatively possible to determine under what deformational type we are by the spatial location of the P/T axes, and even if these have probably varied in time (Fig. 5). In the second place, we should mention the method of the ẏ/R diagram (Armijo, 1977; Simón Gómez, 1982, 1986). By developing Bott's ecuation

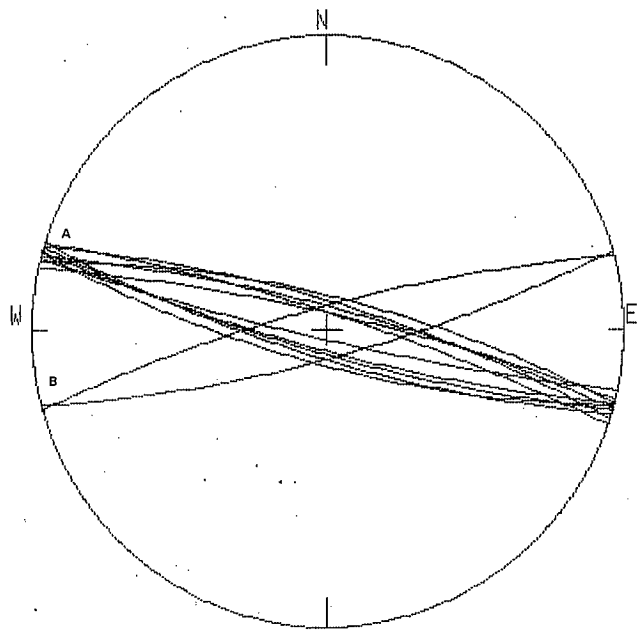

Fig. 3.—Fault cyclographics in a theoretical example. A direction (A) predominates over another one (B). This is a common situation when representing data obtained in the field.

Fig. 3.—Ciclográficas de fallas en un ejemplo teórico. Una dirección (A) predomina mucho sobre otra (B). Esta situación suele ser muy común al representar los datos medidos en el campo.

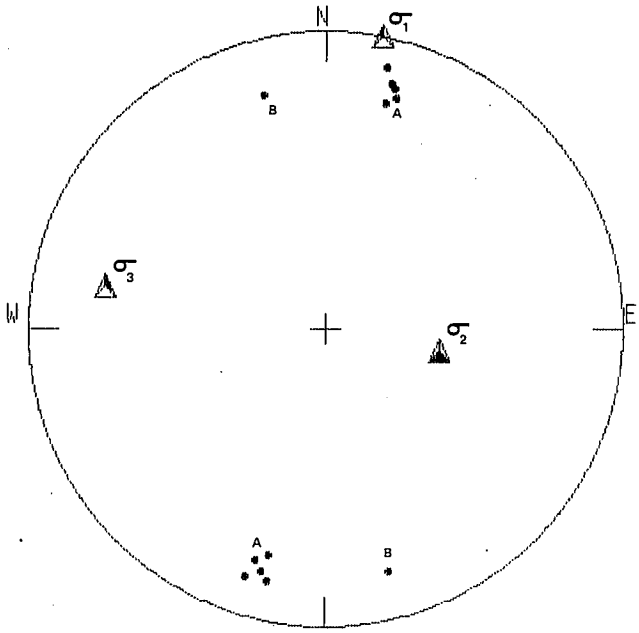

Fig. 4.—Stress directions (triangles) deductible using a method based on the eigenvectors concept. The result does not agree with the minimum dihedral criteria. The data used to apply this criteria are those represented in Fig. 3.

Fig. 4.—Direcciones de esfuerzos (triángulos) deducibles utilizando un método basado en el concepto de autovectores. El resultado no concuerda con el criterio del diedro mínimo. Los datos sobre los que se aplica son los representados en la Fig. 3.

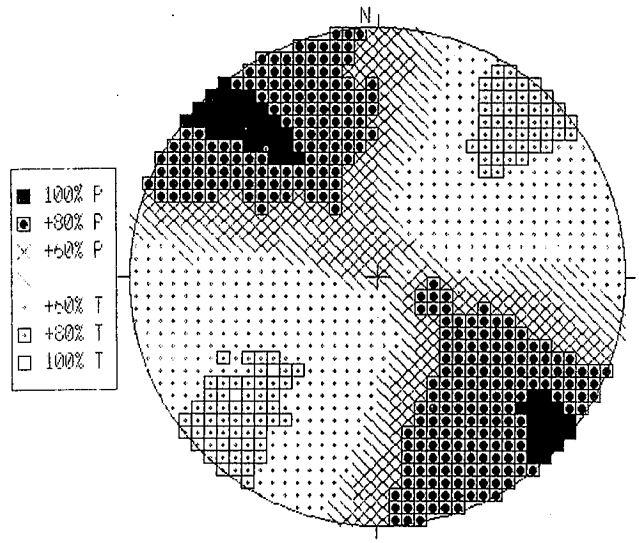

Fig. 5.—Example of density diagram of P/T axis (P compression, T extension) (Angelier and Mechler, 1977). Data treated with program DDEN (de Vicente, unpublished) for 1264 pixels. We appreciate an indefinition in the P axis which seems to vary from vertical to horizontal, although horizontal compression direction is found between N140E and N160E.

Fig. 5.—Ejemplo de diagrama de densidad de ejes P/T (P compresión, T extensión) (Angelier y Mechler, 1977). Datos tratados con el programa DDEN (de Vicente, inédito) para 1264 pixels. Se aprecia una indefinición en el eje P, que parece variar desde encontrarse vertical a horizontal, aunque la dirección de compresión horizontal se encuentra entre los N140E y los N160E.

(1959), it is possible to get another one that relates the invariant of the stress tensor, $R = (\sigma_1-\sigma_2/\sigma_3-\sigma_2)$.

With the striation's pitch, the fault's dip and the maximum horizontal compressive axis (y). In this way, for each fault it is possible to draw a curve as a function of this latter angle and R. The points of the maximum intersection of the curves of a given population will represent compatible places either in this angle (y) as in R. From this method is easy to distinguise among faults that are the answer to different deformational moments, as well as evolutions from ones to the others (Fig. 6).

However, even using this type of methods, or the one that we are going to describe rigth now, it may happen that the fault population is distributed in such a way that, due to the tectonic complexity or the sampling errors, it can be difficult to see clearly the maximum of intersections. In this case, and just in this case, it should be used some type of filtering of structural data to get a valid conclusion (see Appendix 1).

4. THE SLIP MODEL

However, all these methods that obtain the types of ellipsoids, mainly of stress, are initially based in the Anderson's faulting model (1957). Anyhow, Reches (1983) has proposed a new model that although it is not a new faulting theory since it is developed when the different faults start slipping the ones over the others, it gives a new deformation concept in which the role of the intermediate axis is important. This is the «slip model», in which it is proposed that the set of faults slipped during the same tectonic phase is arranged according to an orthorrombic symmetry.

The tests performed by Oertel (1965) and Reches and Dieterich (1983) under three dimensional general deformation ($e_1 \neq e_2 \neq e_3$) show the common presence of four fault sets. According to this model, just in the case of plane strain will appear two sets (Anderson's model). In this regard we should point out that many diagrams coming from very different tectonic situations seem to show clearly the generality of the orthorrombic symmetry produced by one single tectonic phase (Donath, 1962; Aydin, 1977; Brun and Pavlis, 1981; de Vicente *et al.*, 1986; Capote *et al.*, 1986a) either in the microstructural level (Fig. 7) as well as in the macrostructural (Fig. 8) and even related to stresses and strains active today (Fig. 9).

For all this, we think that even being convenient and necessary to expand the laboratory research, there are enought observations to claim the existance of faults with orthorrombic symmetry produced in one single tectonic phase. Even very destacated authors in this field like Angelier, have started using such a symmetry (Gauthier and Angelier, 1985).

From this model, from the symmetry relationships of faults that have moved under the same strain field, it is possible to get, not just the friction angle at the slip moment (Ø), but the shape of the strain ellipsoid by getting the K parameter (e_2/e_1) (intermediate semiaxis / main semiaxis) since:

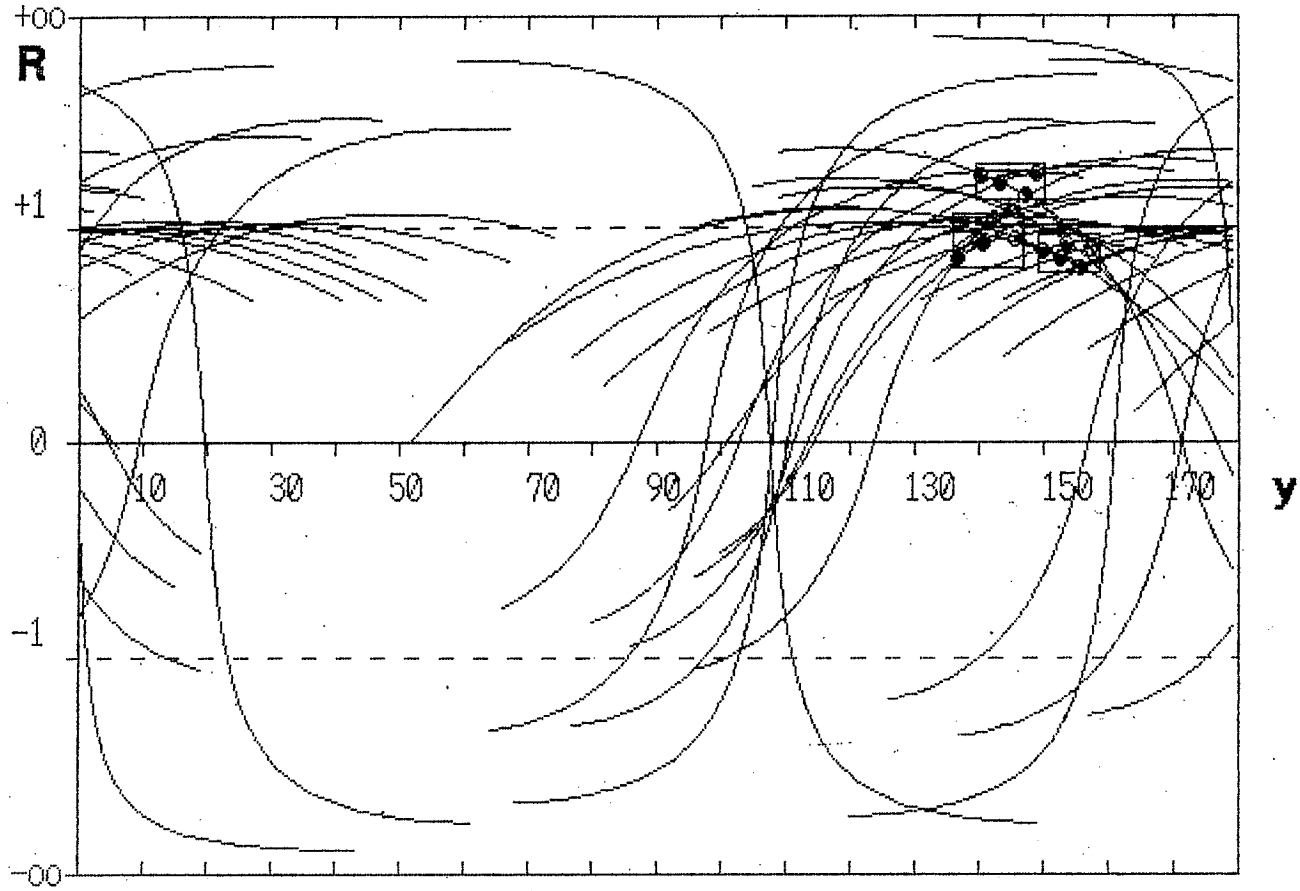

Fig. 6.—Example of y/R diagram (data from Fig. 5). Notice some intersection maximums from R values close to 0,5 (pure strike-slip) going through strike-slip normal faults to normal strike-slip faults (R 1). The deductible compression directions vary between N141E and N154E.

Fig. 6.—Ejemplo de diagrama y/R (los datos son los de la Fig. 5). Se aprecian varios máximos de intersecciones, desde valores de R cercanos a 0,5 (desgarres puros), pasando por desgarres normales hasta fallas normal direccionales (R 1). Las direcciones de compresión deducibles varían entre N141E y N154E.

$$l = \tfrac{1}{2}\,(2/1+K)^{1/2}\,(1-\sin \emptyset)^{1/2} \quad (1)$$

$$m = \tfrac{1}{2}\,(2K/1+K)^{1/2}\,(1-\sin \emptyset)^{1/2} \quad (2)$$

$$n = (\ 2/2)\,(1+\sin \emptyset)^{1/2} \quad (3)$$

For $K \geqslant 0$, since for $-0{,}5 \leqslant K \leqslant 0$

$$l = (\sqrt{2}/2)\,(1-\sin \emptyset)^{1/2} \quad (4)$$

$$m = (\sqrt{2}/2)\,|K|^{1/2}\,(1+\sin \emptyset)^{1/2} \quad (5)$$

$$n = (\sqrt{2}/2)\,(1-|K|)^{1/2}\,(1+\sin \emptyset)^{1/2} \quad (6)$$

Reches, (1983) eqns. (26) and (27). Being l, m, n the director cosines of the faults with respect to the coordinate axes defined by the main strain semiaxes. Therefore, with just the data of trend and dip of the faults it is possible to get directly the orientation and shape of the average strain tensor.

5-K'

The mathematical developement of the «slip model» uses, as we have just mentioned the K factor (e_2/e_1) of the strain ellipsoid; however, taking into account the condition that there is no volume change ($e_3 = -(e_1 + e_2)$) for all kinds of faults, K will vary between 0 and 1 when e_1 and e_2 have the same character, shortening or stretching, and between 0 and -0,5 in the opposite case. The K defined in this way doesn't allow us to distinguish among the different deformational types that are produced in relation to different types of faults. If we define a new factor, K' as the ratio between the maximum horizontal shortening compressive strain axis (or the minimum extensive strain) and the vertical strain axis, ($K' = e_{mxh}/e_v = e_y/e_z$) we will be able to clearly differentiate, between +oo and -oo, 13 different deformational types that can be joined in two sequences. In one hand, the normal sequence (e_z shortening), and on the other, the reverse sequence (e_z stretching) (Table 1).

In Fig. 10 it can be seen a summary of the deformational types described before, and in Fig. 2, related to the development of stylolites and veins.

From eqns. (1), (2), (3), (4), (5) and (6), and taking into account that:

$$l = \sin B \sin D \quad (7)$$

$$m = \sin B \cos D \quad (8)$$

$$n = \cos D \quad (9)$$

Where B is the fault's dip and D is the angle between the fault's trend and e_y (maximum shortening or minimum horizontal stretching semiaxis) if the sequence is normal and between e_y and the trend of the fault's dip if the sequence is reverse.

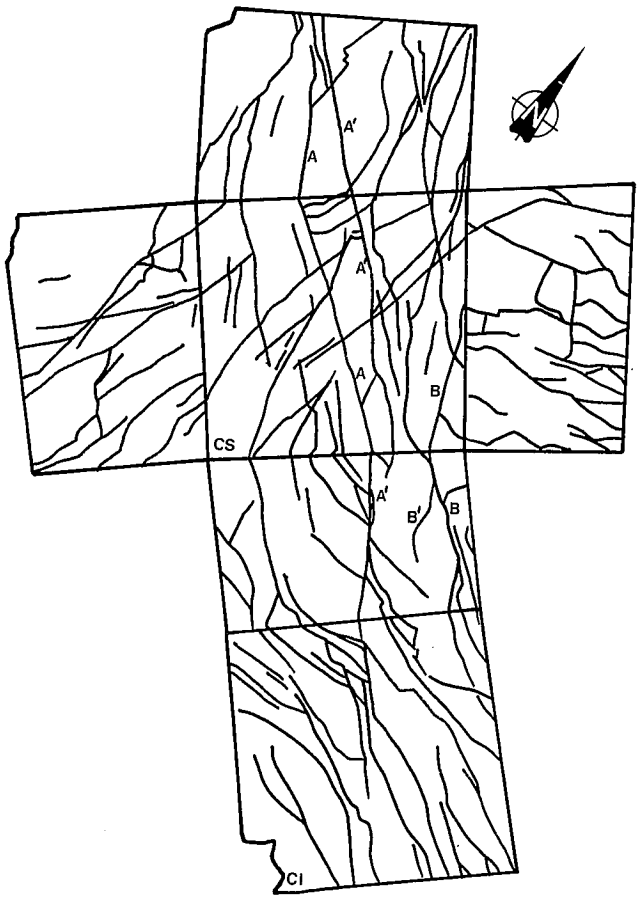

Fig. 7.—Sample of the «Dolomias tableadas de Imon» formation (Iberian Range) in which we can appreciate the four fracture families deductible from the «slip model». A-A' (same trend, opposite dip) and B-B'. CS, upper side. CI, lower side. The sample has 5 cm of side. The fractures are represented in the stereogram of Fig. 19.

Fig. 7.—Muestra de la Formación «Dolomías Tableadas de Imón» (Cordillera Ibérica) en la que se pueden apreciar las cuatro familias de fracturas deducibles del «modelo de deslizamiento». A-A' (igual dirección, buzamiento contrario) y B-B' (idem). CS, cara superior. CI, cara inferior. La muestra tiene 5 cm de lado. Las fracturas son las representadas en el estereograma de la Fig. 19.

It turns to be easy to deduce that for $+oo > K' > 0$ and $-oo < K' < -1$, it means, when there is a substantial directional component,

$$\emptyset = \text{Arcsin}\ ((2\ \sin^2 B\ \cos^2 D)-1) \quad (10)$$

Whereas K' has values within the normal field ($+oo > K' > 0$)

$$K' = \tan^2 B\ \sin^2 D \quad (11)$$

And with a reverse component ($-oo > K' > -1$)

$$K' = -(1 + \tan^2 B\ \sin^2 D) \quad (12)$$

For cases close to radial (either in compression as in extension $0 > K' > -1$), the friction angle is only a function of the dip, whereas K' is a function of D. Then, for normal faults ($0 > K' \geqslant -0{,}5$):

$$K' = -\sin^2 D \quad (13)$$

$$\emptyset = 2B - 90 \quad (14)$$

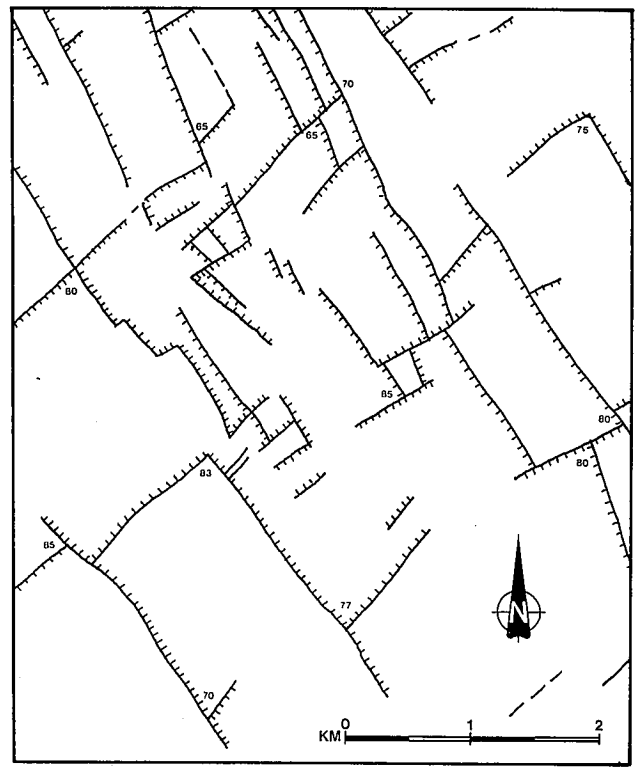

Fig. 8.—Map of faults originated in a radial extension (Millares) graben, S of the Iberian Range) in which we can clearly appreciate the existence of 4 families of contemporary faults (with two opposite directions and dips) (see Appendix 2, figs. 20 and 21).

Fig. 8.—Mapa de fallas originadas en una distensión radial (Fosa de Millares, S de la Cordillera Ibérica) en el que se aprecia claramente la presencia de 4 familias de fallas contemporáneas (con dos direcciones y buzamientos contrarios) (ver Apéndice 2, figs. 20 y 21).

Whereas for the reverse ones:

$$K' = -\cos^2 D \quad (15)$$

$$\emptyset = 90 - 2B \quad (16)$$

This equation set is a very useful tool to be used as a first aproximation to a given study area (see Appendix 2). The graphical representation of this equations (Fig. 11) is very convenient to directly compute the shape of the strain ellipsoid from the K' parameter (as well as the friction angle at the slip moment).

From this diagram a series of interesting consequences can be deduced from the aplication of the «slip model». For the usual types of rocks, with friction angles between 10 and 60 degrees, there shouldn't exist any faults with dips between 40 and 50 degrees (Fig. 11). The reverse faults (s.str.), as they have been defined here, should have dips between 15 and 40 degrees, whereas the normal ones (s.str.) should vary between 50 and 75 degrees. In both cases the radial type of deformation implies a separation angle ($S = 2D$) between faults of 90 degrees, whereas the less radial is the ellipsoid, the smaller the separation angle should be (Fig. 11), until the uniaxial types, in which the separation angle is 0. In the case of faults with a directional component included in the range of $\emptyset$ mentioned before, there shouldn't exist fault sets

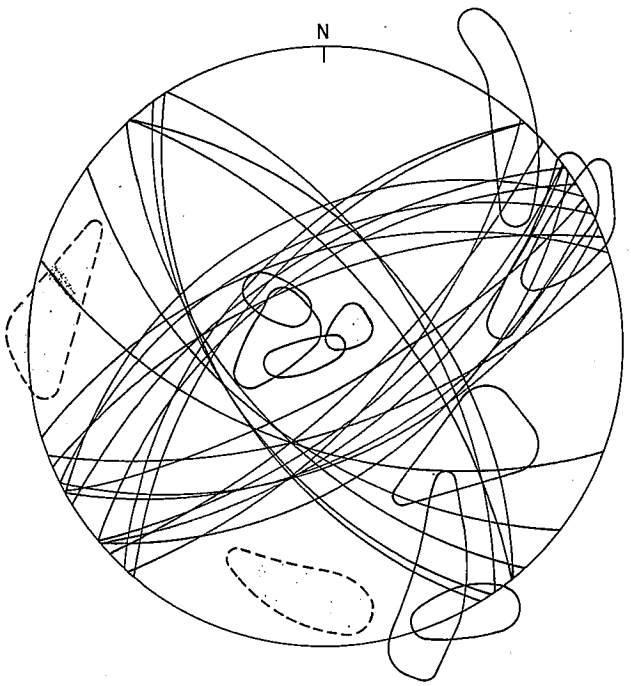

Fig. 9.—Cyclographycs of active faults and in situ measured stresses (Mills *et al.*, 1986), in NW New Zealand. Notice a clear orthorrombic symmetry. From Anderson's model, two orthogonal tensors acting simultaneously were required. This is suggested by the figure because there are two clear concentrations of the experimentally obtained stress directions (open areas), according to the fault directions. However, there is still a measurement which follows the «slip model» (dark areas). If we analyze the relationships between the semiaxes of the stress measurements, we can appreciate that this last data is purely triaxial, while the rest moves near plane strain, probably originated by the presence of active faults. For this reason, the data which follows the «slip model» would represent the regional tensor, which seems to agree with the tectonic trends of the area (Mills *et al.*, 1986).

Fig. 9.—Ciclográficas de fallas activas y medidas de esfuerzos *in situ* (Mills *et al.*, 1986) en el NW de Nueva Zelanda. Se aprecia una clara simetría ortorrómbica. Desde el modelo de Anderson se requerirían dos tensores ortogonales actuando simultáneamente, lo cual parece sugerirse en la fig., ya que aparecen dos claras concentraciones de las direcciones de esfuerzos obtenidos experimentalmente (áreas abiertas), según las direcciones de las fallas. No obstante, aparece una medida que sigue el «modelo de deslizamiento» (áreas oscuras). Si se analizan las relaciones entre los semiejes de las medidas de esfuerzo, puede apreciarse que este último dato es netamente triaxial, mientras que el resto se aproxima a deformación plana, probablemente originada por la presencia de fallas activas, por lo que, en este caso, el dato que sigue el «modelo de deslizamiento» representaría el tensor regional, lo que parece estar de acuerdo con las directrices tectónicas de la zona (Mills *et al.*, 1986).

Table 1

	$K' = +oo$	STRIKE-SLIP (plane strain)	$(e_z = 0.\ -e_x = e_y)$
NORMAL	$+oo > K' > 1$	STRIKE-SLIP NORMAL	$(-e_x > e_y > e_z)$
	$K' = 1$	—	$(-e_x > e_y = e_z)$
	$1 > K' > 0$	NORMAL STRIKE-SLIP	$(-e_x > e_z > e_y)$
	$K' = 0$	(plane strain)	$(-e_x = e_z.\ e_y = 0)$
	$0 > K' > -.5$	NORMAL (s.s)	$(e_z > -e_x > -e_y)$
	$K' = -.5$	(radial extension)	$(e_z > -e_x = -e_y)$
	$K' = -.5$	(radial compression)	$(-e_z > e_x = e_y)$
REVERSE	$-1 < K' < -.5$	REVERSE (s.s)	$(-e_z > e_y > e_x)$
	$K' = -1$	(plane strain)	$(-e_z = e_y.\ e_x = 0)$
	$-2 < K' < -1$	REVERSE STRIKE-SLIP	$(e_y > -e_z > -e_x)$
	$K' = -2$	—	$(e_y > -e_x = -e_z)$
	$-oo < K' < -2$	STRIKE-SLIP REVERSE	$(e_y > -e_x > -e_z)$
	$K' = -oo$	STRIKE-SLIP (plane strain)	$(e_y = -e_x.\ e_z = 0)$

with separation angles greater than 80 degrees even though the dip is what mainly controls the type of K', showing a general trend both in the normal faults sequence and in the reverse ones to increase the directional component as the dip increases. This effect is more important if the separation angles are small.

In relation with the radial regimes and the friction angle, we can deduce that if it decreases with depth, the normal faults should show a listric geometry, what means lower dip with depth whereas the opposite situation should happen in the case of reverse faults.

The difference between «normal sequence» and «reverse sequence» is very important to interpret the type of ellipsoid that causes the deformation, mainly in the limit cases ($K' = oo$). Under deformational regimes close to pure strike-slip the coexistence of slightly reverse strike-slip faults (e_z sligthly stretching, $K' \approx -oo$) and slightly normal ($K' \approx +oo$, e_z sligthly shortening) may happen. This would produce the presence of four faulting directions, two of them showing in their minimum dihedral (minimum dihedral of the dip directions). This fact seems to be very common in strike-slip tectonics, for instance, Capote *et al.*, (1986a) show that this is the type of current tectonics in the Alboran Sea area (South of Spain). On the other hand, in the experiments carried out by Barlett *et al.*, (1981) under deformational conditions close to pure strike-slip (plane strain, $K' \approx oo$), within the shear bands and as a response to a local deformational field between a series of «Y» planes (Fig. 12) four fracturation directions show up; two of them, the traditional «R» and «R'» are the consequence of a slightly normal tensor, whereas the «X» and «P» correspond to slightly reverse strike-slip.

Therefore, from the concept of K' and the «slip model», either regional tectonic situations, as well as experimentally found microfracture sets in disagreement with Anderson's fraturation theory are explained.

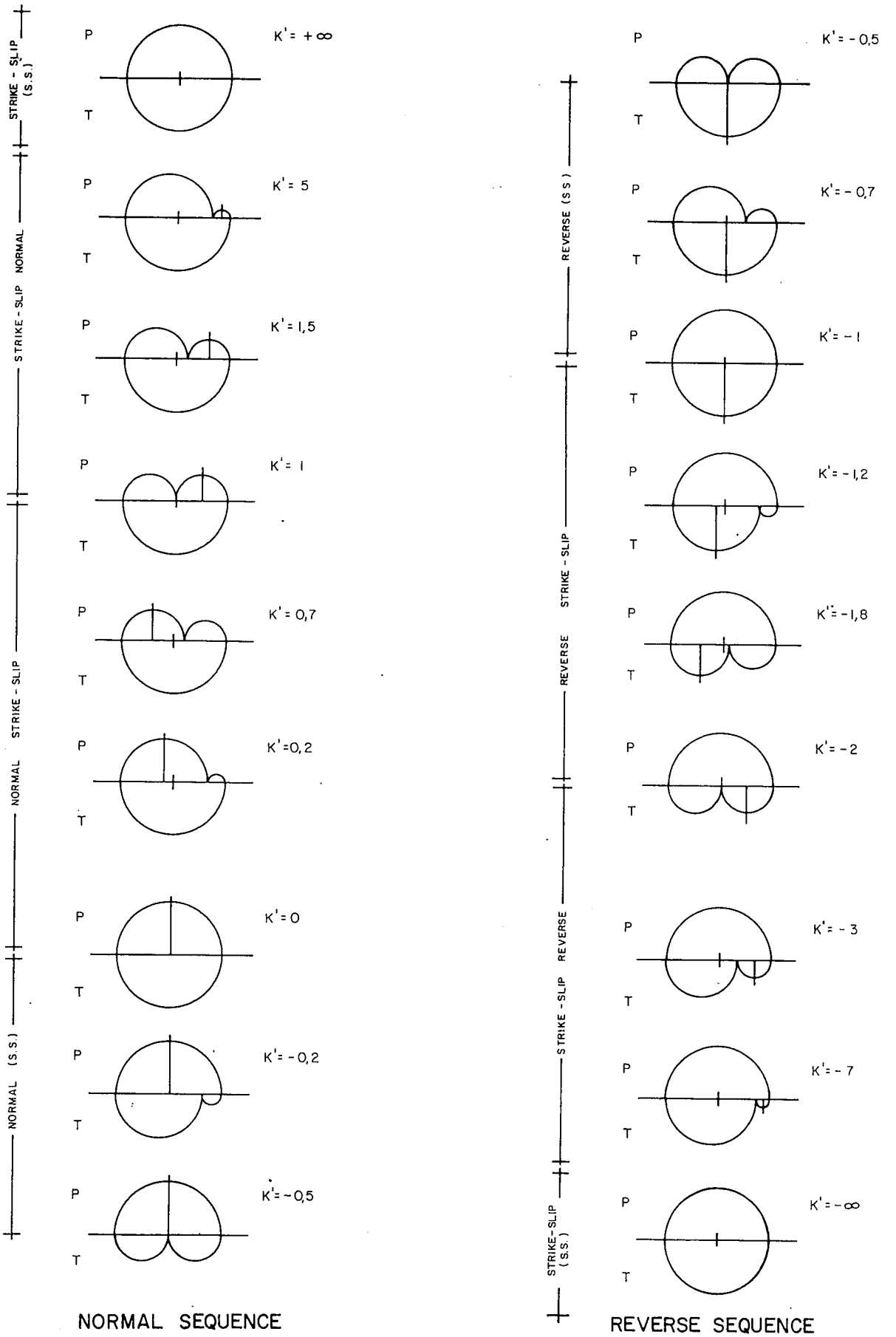

Fig. 10.—Graphical representation of the different deformational types defined by K' (see table in text). P, shortening ($e < 0$), T stretching ($e > 0$). The bar indicates which of the three axes corresponds to e_z (vertical).

Fig. 10.—Representación gráfica de los distintos tipos deformacionales definidos por K' (ver tabla en el texto). P acortamiento ($e < 0$), T alargamiento ($e > 0$). La barra indica cual de los tres ejes es el que corresponde a e_z (vertical).

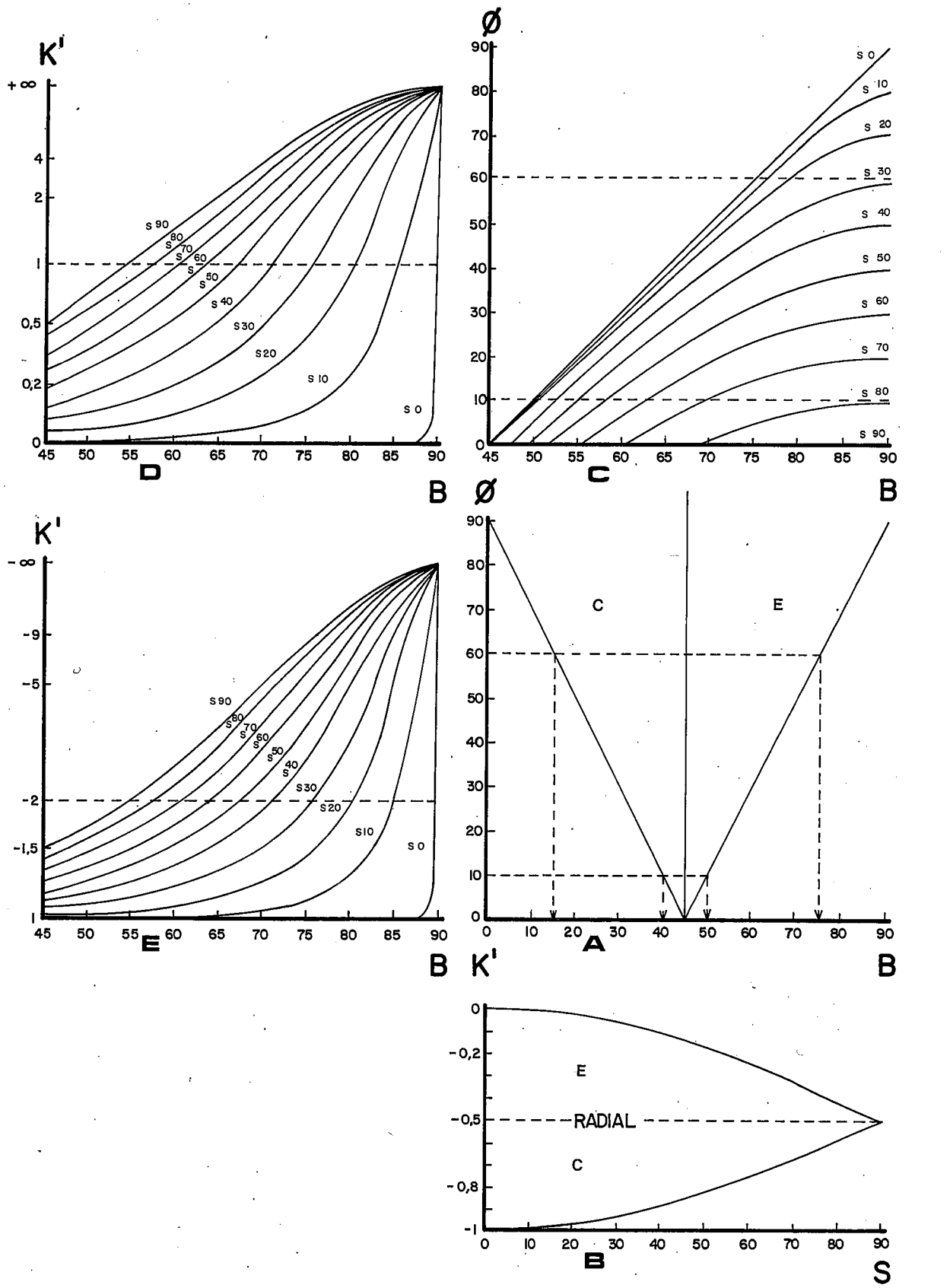

Fig. 11.—A) Relationships between Ø and the dip of the fault (B), and B) between K' and S (separation angle between faults), for radial regimes (0 >K' >-1) deductible from the «slip model». (C shortening, E stretching).
Relationships between Ø and K' with the dip (B) and the separation angle between faults (S) in not radial regimes. C) Ø for normal and reverse sequences. D) K' for normal sequence. E) K' for reverse sequence.

Fig. 11.—A) Relaciones entre Ø y el buzamiento de las fallas (B), y B) entre K' y S (ángulo de separación entre las fallas), para regímenes radiales (0 >K' >-1) deducibles del «modelo de deslizamiento» (C acortamiento, E estiramiento).
Relaciones entre Ø y K' con el buzamiento (B) y el ángulo de separación entre las fallas (S) en caso de regímenes no radiales. C) Ø para las secuencias normal e inversa. D) K' en la secuencia normal. E) K' en la secuencia inversa.

6. THE e/K' DIAGRAM

Coming back to the ideas exposed in the begining of this paper, from the existing relationships among K', Ø, D and B a few statistical methods could be developed. However, as we mentioned, is preferable to use one in which we don't lose the singularity of each data. From each measured fault in the outcrop, we know initially its trend and dip. If we can estimate to which of the two main sequences it belongs, either from indicators displacement, from the type of striations, or from the considerations that we have just done related to the dip, we'll know that, in the case of the normal sequence, the main horizontal shortening semiaxis (e_y), or the less extensive one won't be farther than 45 degrees to either side of the fault trend, whereas if we are in the reverse sequence, the maximum horizontal shortening axis will be no farther than 45 degrees from the dip's trend of the fault. If we draw the curves, 45° to both sides that related K' as a function of B and D for each fault, for a given fault population, we will get its corresponding curve population, that is denominated e/K' diagram (Fig. 13). From a diagram of this type, a series of interesting conclusions can be withdrawn. In the case of the normal sequence, when the separation angle is equal to zero, it means, when D = 0 (this implies that the considered semiaxis direction is parallel to the fault's trend and that the deformation should be plane), K' takes the value of 0, then, each curve from each fault will take a symmetric shape with a pike of K' = 0 coincident with its trend. Taking into account the minimum dihedral criteria, the trend of the semiaxis will be at the minimum angle that two different sets of pikes form, coinciding with a maximum at the intersections of the two curve sets so generated, getting in the same way the value of K' (Fig. 13). The same thing can be said for the reverse sequence, but in this case the pikes are located at -1 (plane deformation) and D corresponds with the trend of the dip of the fault (Fig. 14).

This is valid just in the case that the population under study corresponds to a single tectonic event. In the case that the faults are produced in several deformational stages we will have at least so many maximums as phases; probably more because of the random intersections. In this case, we have to differentiate the real maximums with field criteria and from the shape of the curves in the same diagram. This means that we shouldn't take into account the intersections between curves of different wavelength and intersections with incompatible separation angles.

The method turns to be very interesting to study the evolutions of the strain with time. As it has been shown (Simón Gómez, 1983, 1986; Guimera, 1986; Capote *et al.* 1986b), the transit from the last compression to the first extension in the Iberian Range (E of Spain) was gradual, keeping the orientation of the stress and strain axes, but changing the main compressive one from horizontal to vertical. A typical e/K' diagram for this transit is shown in Fig. 15. It can be seen that, whereas the areas of pikes of K' = 0 are kept, and then the values of the maximum horizontal shortening direction (e_y), there are several intersection points of K' with different values.

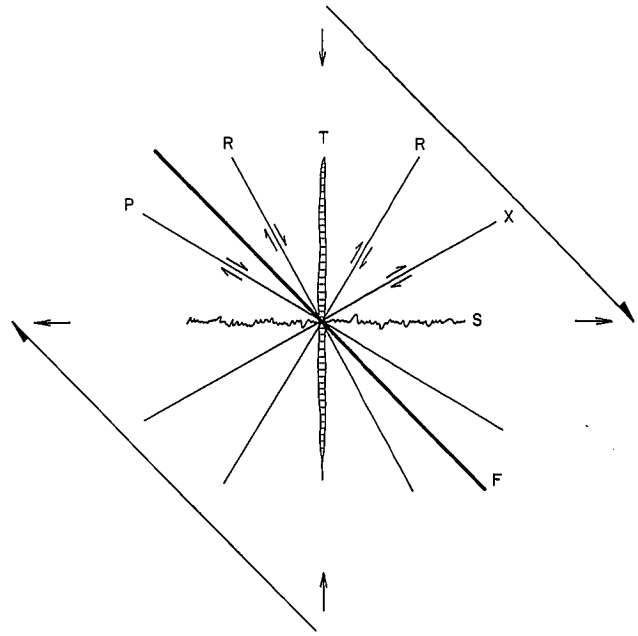

Fig. 12.—Explanation of secondary fractures in a shear zone from the «slip model». R and R' would be slightly normal strike-slip faults, whereas X and P would also be strike-slip faults but slightly reverse (F, main fault plane, T, tension fissure and S, stylolite).

Fig. 12.—Explicación de las fracturas secundarias de una zona de cizalla desde el «modelo de deslizamiento». R y R' serían desgarres ligeramente normales, mientras que X y P serían igualmente desgarres pero ligeramente inversos. (F, plano de falla principal, T, grieta de tensión y S estilolito).

With the same basis as in the e/K' diagram, the e/Ø diagram can be made representing in this case the variation between Ø and D. With the same data that show variation in the deformation ellipsoid, we get in this case the diagram shown in Fig. 16. Only one maximum of the value of Ø can be appreciated, which is logic because it is the same kind of material and there was little variation in the deformation conditions during the considered period of time, with a maximum horizontal deductable compression direction similar to the one given by the e/K' diagram (Fig. 15).

The programming of the method is not difficult, in our case it was been carried out by means of the program DEK (de Vicente, unpublished) in MFBASIC.

7. COMBINATION OF METHODS

When studying the brittle tectonics of a given area, however the most profitable strategy is to use kinematic markers as well as a series of independent populational analysis methods. In this way, in the area represented by the diagrams in figs. 15 and 16, the corresponding diagrams e/K' and y/R modified so they obbey the «slip model» and the location of stylolytes and veins (figs. 5, 6 and 17) give us similar results, with a small degree of error.

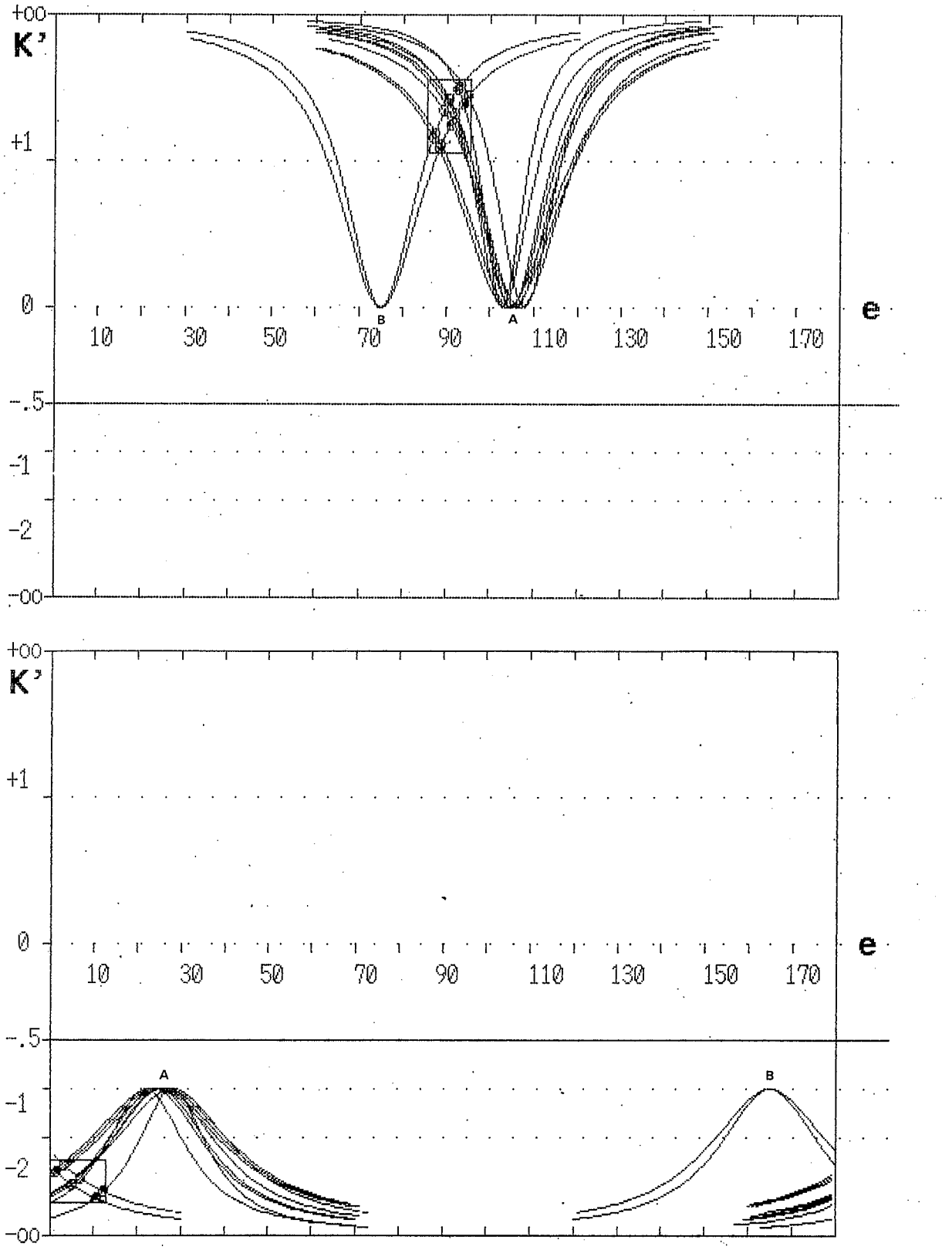

Fig. 13.—Example of e/K' diagram based on data of Fig. 3. We appreciate that unlike the method based on eigenvectors (Fig. 4), the shortening direction is deducible following the minimum dihedral criteria (normal sequence).

Fig. 13.—Ejemplo de diagrama e/K'. Los datos sobre los que se aplica son los de la Fig. 3. Se aprecia que, a diferencia del método basado en autovectores (Fig. 4), la dirección de compresión deducible sí sigue el criterio del diedro mínimo (secuencia normal).

Fig. 14.—The same example as in Fig. 13 but considering the reverse sequence (The resulting shortening directions are orthogonal).

Fig. 14.—El mismo ejemplo de la Fig. 13, pero considerando la secuencia inversa (las direcciones de compresión resultantes son ortogonales).

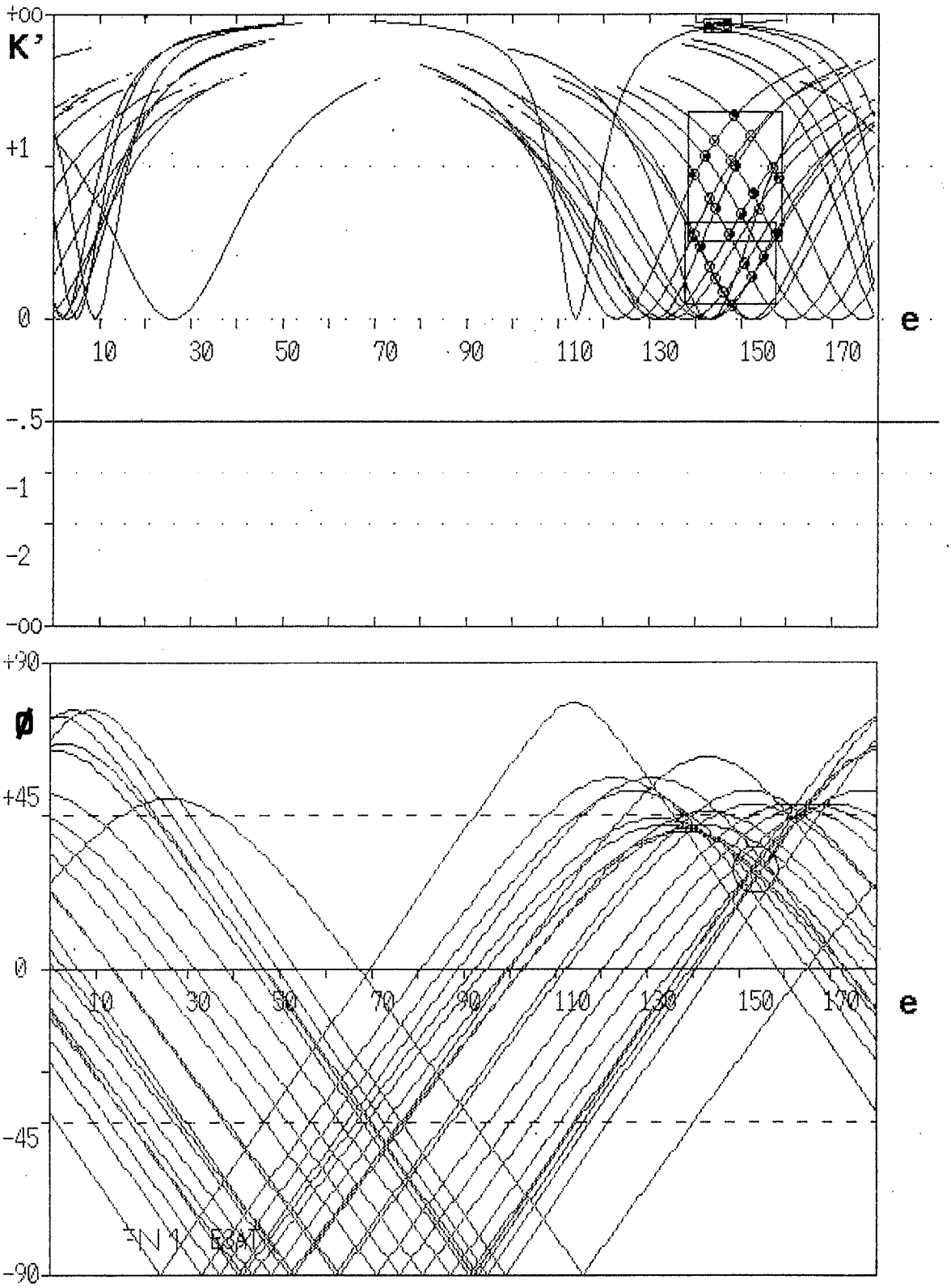

Fig. 15.—Example of continuous variation of the type of K' from nearly pure strike-slip (K' = + oo) to normal strike-slip faults, keeping fixed e_y direction (N138E to N157E). Data are the ones already seen in Fig. 5 for P/T diagram and in Fig. 6 for y/R diagram. We appreciate coherence in the results obtained from the three methods. The station is placed SE of Sigüenza (Castillian Branch, Iberian Range).

Fig. 15.—Ejemplo de variación continua del tipo de K', desde desgarres casi puros (K' = + oo) hasta fallas normal direccionales, manteniéndose fija la dirección de e_y (N138E a N157E). Los datos son los ya tratados en la Fig. 5 mediante el diagrama P/T y en la Fig. 6 por el diagrama y/R. Se aprecia la congruencia en los resultados de los tres métodos. La estación se encuentra situada al SE de Sigüenza, rama Castellana de la Cordillera Ibérica.

Fig. 16.—e/Ø diagram for the data in preceding figure; while we could appreciate several values of K', here we can see just one maximum value for Ø (29 degrees) with a shortening direction of N154E.

Fig. 16.—Diagrama e/Ø para los datos de la figura anterior mientras que allí se apreciaban varios valores de K', aquí se observa un único valor de Ø (29 grados), con una dirección de compresión de N154E.

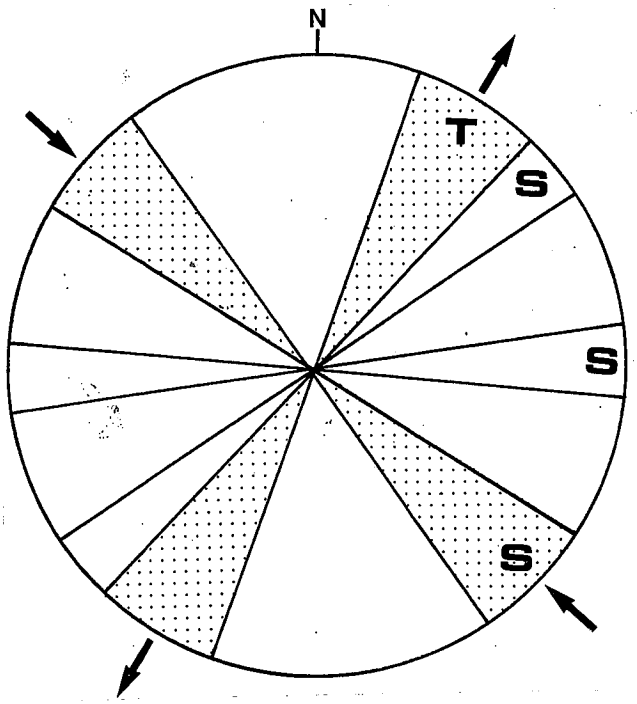

Fig. 17.—Diagram of predominant directions of stylolites (S) and veins (T) in the area representing figs. 5, 6, 15 and 16 (dotted areas represent stylolites and veins corresponding to the described deformation state).

Fig. 17.—Diagrama de direcciones predominantes de estilolitos (S) y venas (T) en el área que representan las Figs. 5, 6, 15 y 16 (en punteado se han marcado los estilolitos y las venas correspondientes a la fase de deformación descrita).

Despite all this and even if some combined methods are used, data obtained in field geology are essential.

8. CONCLUSSIONS

— In populational analysis of faults, the use of statistical methods in which the singularity of each data does not get lost as in the P/T, y/R modified or the proposed e/K' diagrams is very convenient.

— Kinematic indicators represent a great help to know the brittle tectonics of a given region, althrough when taking into account the role of the intermediate axis, its spacial relationships are more complicated than the exposed up to now.

— We think that the «slip model» is very useful in laboratory work as well as for field data.

— Thirteen different deformational types between $K' = +\infty$ and $K' = -\infty$ are described related to the K' (e_y/e_z) factor.

— A series of equations and their corresponding e/K' and e/Ø diagrams are deduced. From the trend and dip of the faults is then possible to know the orientation and change in deformational type of tensor evolutions.

The advantages of this method are its easy use, its speed of calculus and, mainly, the no dependency of the weight of each of the present families.

AKNOWLEDGEMENTS

I want to thank Eugenia Fierros and Dr. Jesús Tenajas for the translation of the manuscript. Also to Pedro J. Vicente for drawing the figures.

Finally, to Dr. Ramon Capote for his great help and advice for making possible the completion of this research, which has been partially supported Pproject N.3394 C.A.I.C.Y.T. «El Lias de la Rama Nororiental de la Cordillera Ibérica».

REFERENCES

Aleksandrowski, P. (1985): Graphical determination of principal stress directions for slikenside lineation populations. *Jour. Struct. Geol.*, 73-82.

Anderson, E.M. (1951): *Dynamics of faulting.* Oliver and Boyd. Edinburg, 206 p.

Angelier, J. and Mechler, P. (1977): Sur une methode graphique de recherche des contraintes principales egalement utilisable en tectonique et en seismologie: La methode des diedres droits. *Bull. Soc. Geol. France,* XIX, (7), 1.309-1.318.

Armijo, R. (1977): *La zone de failles de Lorca-Totana (Cordilleres Betiques, Espagne). Etude tectonique et neotectonique.* These Doct., Univ. Paris VII, 98 p.

Arthaud, F. (1969): Methode de determination graphique des directions de raccourcissement, d'allongement et intermediaire d'une population de failles. *Bull. Soc. Geol. France* (7), 11, 729-737.

Aydin, A. (1977): *Faulting in sandstone, Utah.* Ph. D. Diss., Stanford Univ., Calif.

Barlett, W.L., Friedman, M. and Logan, J.M. (1981): Experimental folding and faulting of rocks under confining pressure. Part IX, wrench faults in limestone layers. *Tectonophysics,* 79, 255-277.

Bott, M.H.P. (1959). The mechanics of oblique slip faulting. *Geol. Mag.,* 96, 109-117.

Bruhn, R.L. and Pavlis, T.L. (1981). Late Cenozoic deformation in the Forearc region: Matanuska Valley, Alaska: three-dimensional strain in a forearc region. *Geol. Soc. Amer. Bull.,* 92, 282-293.

Capote, R., de Vicente, G., González Casado, J.M., and González Vallejo, L. (1986a): Análisis de los elipsoides de esfuerzo y deformación de la tectónica actual en la región de Alborán a partir del análisis poblacional de los mecanismos focales de terremotos. *I Jorn. Est. Fenom. Sísmico. Murcia.*

Capote, R., de Vicente, G., González Casado and J.M. Fernández, C. (1986b): *Estudio neotectónico de los alrededores de la presa de Tous* (unpub.).

de Vicente, G. (unpub.): Programa FILCO7.

de Vicente, G. (unpub.): Programa DEK'.

de Vicente, G., Martínez, J., Capote, R. and Lunar, R. (1986): Determinación de los elipsoides de esfuerzo y deformación asociados a la mineralización argentifera de Hiendelaencina (Sistema Central). *Estudios Geol.,* 42, 23-31.

Donath, F.A. (1962): Analysis of basin-range structure, South-Central Oregon. *Geol. Soc. Amer. Bull.,* 73, 1-16.

Hancock, P.L. (1985): Brittle microtectonics: principles and practice. *Jour. Struct. Geol.*, 7, 3/4, 437-457.

Gauthier, B. and Angelier, J. (1985): Fault tectonics and deformation: a method of quantification using field data. *Earth Planet. Sci. Lett.*, 74, 137-148.

Guimera, J. (in press): Precisiones sobre la estructura y la edad de las deformaciones en el área de Llucena-Ribesalbes (Prov. de Castellón de la Plana). *Bol. Geol. Min.*

McKenzie, D.P. and Jackson, J.A. (1983): Thickening, paleomagnetism, finite strain and fault movements within a deforming zone. *Earth Planet. Sci. Lett.*, 65, 182-202.

Mills, K.W., Pender, M.J., Depledge, D. (1986): Measurement of in situ stress in coal. *Proc. Int. Symp. Rock Stress and Rock Stress Measurements.*

Oertel, G. (1965): The mechanism of faulting in clay experiments. *Tectonophysics,* 2, 343-393.

Reches, Z. (1983): Faulting of rocks in three-dimensional strain fields. I Failure of rocks in polyaxial, servo-control experiments. *Tectonophysics,* 95, 111-132.

Simón Gómez, J.L. (1982): *Compresión y distensión alpinas en la cadena ibérica oriental.* Tesis Doct., Univ. Zaragoza. 269 pp.

Simón Gómez, J.L. (1986): Analysis of a gradual change in stress regime (example from the eastern Iberian Chain, Spain). *Tectonophysics,* 124, 37-53.

APPENDIX 1

Due to sampling errors and to the normal dispersion of microstructural data, the population distribution can make difficult to try any latter interpretation. This is the reason why, in these cases, we will have to use some kind of filtering technique. It is obvious that in this way we lose the singularity of each data, but in a rational way, with «soft» filters, studies in areas with the described problems can be successful.

The are some ways to filter. We propose one based on the confidence cones concept summarized in the organigram in Fig. 18, which is easy to program (in our case have program FILCO 7, De Vicente, (unpub.), in MBASIC). In this way, data as in Fig. 19a, can be «cleaned» to get Fig. 19b in which we can appreciate much more the predominant trends and dips.

APPENDIX 2

Regional deformation studies can be conduced using equations 12-16, or using diagrams in fig. 11. In this way, if for instance, we suspect that one region has undergone a compression or an extension close to radial, we will be able to estimate, with aerial photograph or satellite imagery, the kind of deformation ellipsoid which produced the faults knowing only the medium separation angle among present fault families (average separation angle S, S = 2D). In the most general case, we will have to know the average separation angle and dip.

The Bicorp-Navarres-Millares system of grabens (located in the south of the Iberian Range) was formed during a radial extension in the upper Miocene-lower Pliocene. From a map of the faults of this phase (Fig. 8) it's possible to extract the separation angle S between each pair of faults. With that and with eq. 13 or the diagram shown in Fig. 11, we can draw a

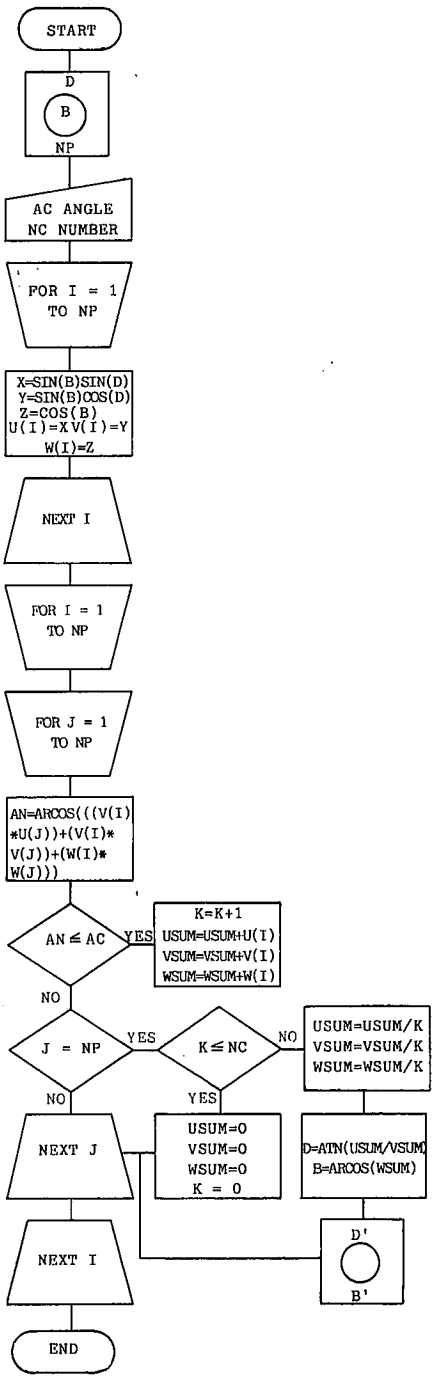

Fig. 18.—Flow diagram of program FILCO7 (de Vicente, unpub.) to filter directional data. The bias are controlled by angle AC (cone opening) and the number NC (minimum number of data which a given data has to have in its surroundings within the AC angle). The number of the data located closer than AC are searched by iterative means. If this number is higher then NC, the average data for each concentration has to be found. The results can be seen in figs. 19 A) and 19 B).

Fig. 18.—Organigrama de flujo del programa FILCO7 (de Vicente, inédito) para el filtrado de datos direccionales. Los pasos de banda se controlan mediante el ángulo AC (apertura del cono) y el número NC (número de datos mínimo que ha de tener alrededor un dato cualquiera a un ángulo menor que AC). Para cada dato direccional se busca, mediante flujos iterativos, el número de otros datos que quedan a distancias menores que AC. Si este número es mayor que NC, se halla el dato medio para cada concentración. Los resultados pueden verse en las figs. 19 A) y 19 B).

contour map of the values of K' (Fig. 20) in which we can appreciate a series of areas with extensions more or less radial (K' = -0.5, radial extension. K' = 0, uniaxial extension) that follow E-W or N100 and N-S or N10 trends. The area of less radial deformation (K' = -0.35) coincides with higher faulting density (Fig. 8).

Taking into account the minimum dihedral criteria and from the symmetry proposed in the «slip model», it is also possible to make a paleodeformation directions map (Fig. 21) (but just of trends, not intensity). We can see that the less radial extension area coincides with a ESE direction and that the limits of that area follow the paleodeformation trends.

In this way and from this easy kind of analysis we can get a series of relationships among directions and types of deformation ellipsoid not possible to get up to now.

Recibido el 30 de abril de 1987
Aceptado el 21 de junio de 1987

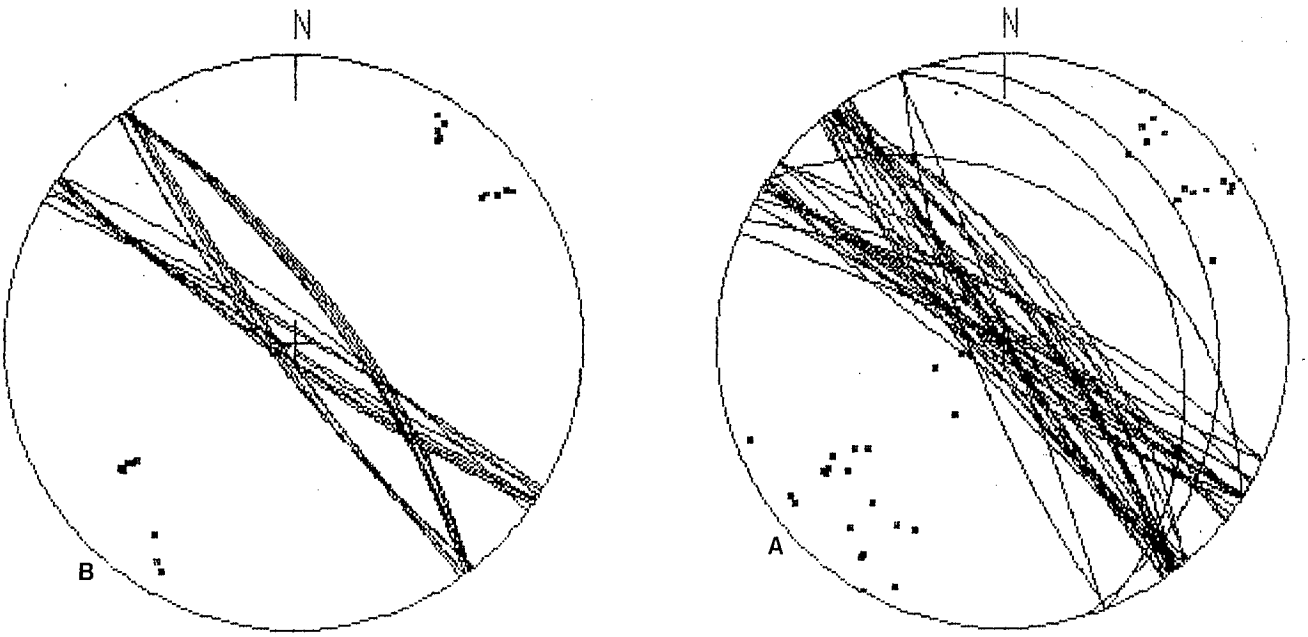

Fig. 19.—A) Example of not filtered data. The measurements correspond to the dolomite cube represented in Fig. 7. B) Data in Fig. 19 A) filtered with the program FILCO 7 (Fig. 18). The main present directions and average dips can be more neatly appreciated (AC = 10°. NP = 2).

Fig. 19.—Ejemplo de datos sin filtrar. Las medidas corresponden al cubo de dolomía representado en la Fig. 7. B) Los datos de la Fig. 19 A) filtrados con el programa FILCO7 (Fig. 18). Se aprecian con mayor nitidez las principales direcciones y buzamientos medios presentes (AC = 10°. NP = 2).

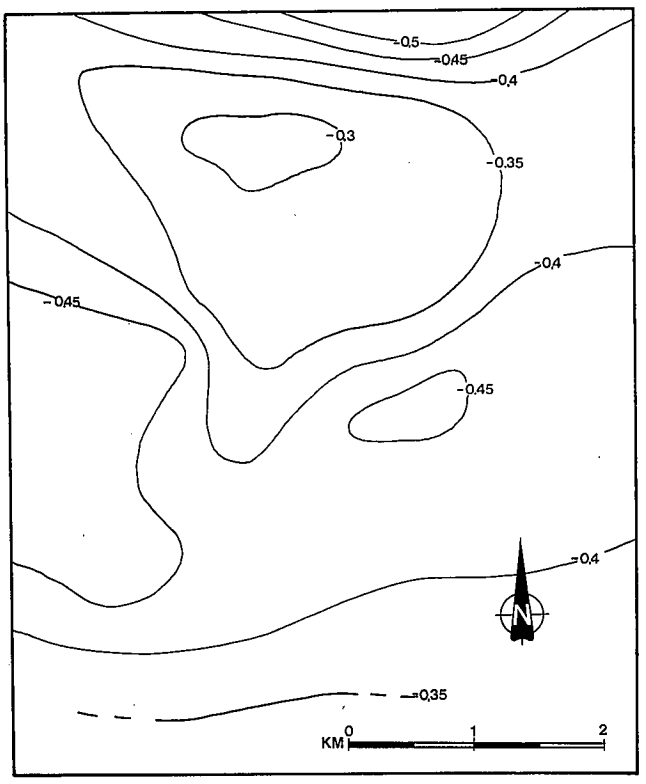

Fig. 20.—Contour map of K' in the area represented in Fig. 8.

Fig. 20.—Mapa de contornos de isovalores de K' en el área representada en la Fig. 8.

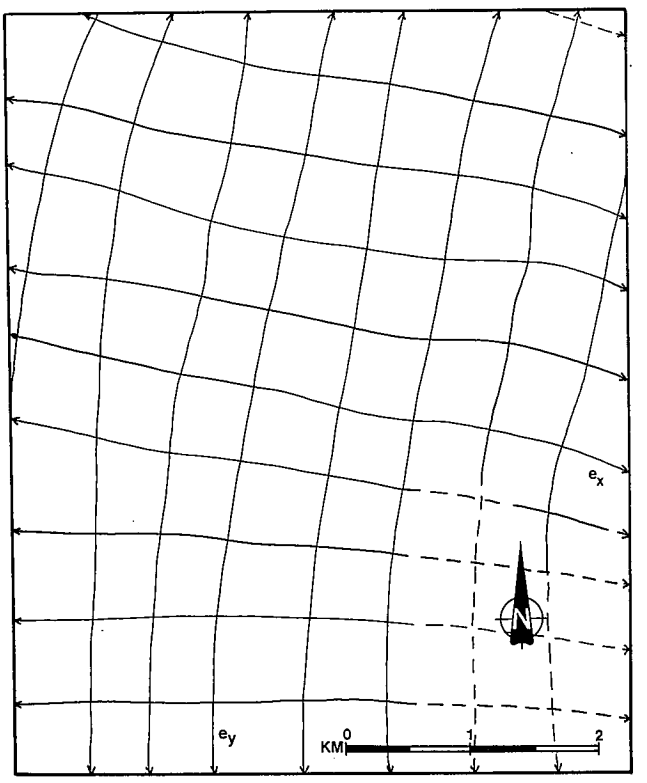

Fig. 21.—Map of paleodeformation trends corresponding to figs. 8 and 20.

Fig. 21.—Mapa de direcciones de paleodeformaciones correspondiente a las figs. 8 y 20.